# Explosive Textural Polarization and Nonequilibrium Phase Transitions in Superfluid $^3$He-$A_1$

P. G. N. de Vegvar,* K. Ichikawa,† and H. Kojima
*Serin Physics Laboratory, Rutgers University, Piscataway, New Jersey 08854*
(Received 23 December 1998)

Anomalous second sound spectra have been observed in a doubly excited rectangular cavity filled with superfluid $^3$He-$A_1$. These include sudden, large, and hysteretic shifts of resonance frequencies. Numerical computations based on $A_1$-phase hydrodynamics show that first order, nonequilibrium, counterflow driven, textural transitions are occurring where the $\hat{\boldsymbol{l}}$ texture abruptly polarizes along the direction of greatest counterflow throughout most of the cavity. Fair agreement is obtained without adjusting any parameters.

PACS numbers: 67.57.–z, 05.45.–a, 47.70.–n, 67.65.+z

The hydrodynamics of systems displaying broken symmetries is currently of much interest to physicists. Recent studies range from collective modes in Bose-Einstein condensed gases to turbulence in Rayleigh-Bénard flows. Superfluid $^3$He occupies a unique niche within this field. Its bulk properties have been intensively investigated over the years, and the nature of its broken symmetries and spin triplet, $p$-wave order parameter is fairly well understood [1]. Here we explore the rich nonlinear interplay between the ac superflow induced by spin-entropy waves in $^3$He-$A_1$ (better known as second sound) and the orientation of the orbital vector component $\hat{\boldsymbol{l}}$ of the order parameter (the texture). We have discovered unexpected and dramatic spectral features in a doubly excited second sound resonator. The measurements are in semiquantitative agreement with nonlinear superfluid hydrodynamics that associates the observed large sudden shifts of the resonance frequencies with first order, nonequilibrium, textural phase transitions. These are bifurcations where the steady-state texture *explosively* polarizes along the larger of two ac counterflows generated by the second sound waves. This is surprising since one intuitively expects the steady-state texture and velocities to vary *continuously* with the excitation conditions. Our studies demonstrate the first controllable ac flow-driven textural transformations in $^3$He-$A_1$. These results have a larger context within condensed matter physics. The flow-induced polarization we observe is an example of a nonequilibrium phase transition like those in turbulence. Second sound has applications in the rapidly developing area of Bose-Einstein condensation and is important in other new superfluids with broken symmetries.

The spin-entropy wave propagation chamber was a rectangular room 9.3 mm $\hat{\mathbf{x}} \times$ 7.2 mm $\hat{\mathbf{y}} \times$ 8.3 mm $\hat{\mathbf{z}}$. Each wall was fitted with a capacitively coupled, dc voltage biased oscillating superleak transducer (OST), whose active member was a stretched, metallized membrane having pores with 3 $\mu$m nominal diameter. The three transducer pairs allowed simultaneous measurement of nonoverlapping modes propagating in all three orthogonal directions. The resonator and a packed Ag powder heat exchanger was placed into a $^3$He-filled can, which lay inside the bore of a superconducting magnet. The $^3$He was cooled into the superfluid $A_1$ phase by independent demagnetization of $PrNi_5$. A magnetic field of 35 kOe along $\hat{\mathbf{z}}$ produced an $A_1$ phase width of 170 $\mu$K at our working pressure of 22 bars. The modes propagating along $\hat{\mathbf{z}}$ obeyed linear response [2].

This cell was designed to measure the change in the response of one transducer pair as the texture was altered by another pair, instead of just detecting the nonlinear response of a single pair [3]. For example, the frequency spectrum of the mode along $\hat{\mathbf{x}}$ was acquired using $\hat{\mathbf{x}}$ transducers while controlling the ac superflow along $\hat{\mathbf{y}}$ by a $\hat{\mathbf{y}}$ transducer. As shown in Fig. 1, a spectrum was taken for each value of $x$- and $y$-drive amplitudes and fixing the $y$ frequency at 123 Hz, sweeping $x$-drive frequency $f_x$ up through the cell's lowest $x$ resonance. This was performed at successively larger $y$ drives, keeping the $x$-drive amplitude fixed. Panels A and B show the in-phase and quadrature responses as $f_x$ was swept at 0.1 Hz/s in the absence of $y$ excitation. It is clear that this $\hat{\mathbf{x}}$-drive amplitude was sufficient by itself to induce a nonlinear response [3]. There was little spectral change up to a threshold $\hat{\mathbf{y}}$-drive amplitude. Panels C and D show the dramatic spectral changes upon exceeding this threshold. We define the "$x$-resonant frequency" as the $f_x$ where the in-phase signal changes sign. Here $x$ resonance increased by 13.5 Hz, about 7 times the resonance width, when increasing the $y$ drive through such a "$y$ jump." Simultaneously the quadrature response vanished into the noise floor.

Figure 2 presents the measured textural phase diagram. For each value of $x$ excitation, expressed as peak-peak ac drive times dc bias voltage, we plot the $y$ excitation where the $y$ jump occurred on raising the $y$-drive amplitude. Averaged data are shown, the scatter being $\pm(10-15)\%$. The transition could be crossed by fixing $x$ drive and raising $y$ drive, or vice versa; the same boundary was obtained. The transition showed hysteresis on reversing the crossing direction, consistent with a first order transformation.

We have undertaken simulation studies to gain further insight into these unexpected findings. The measured cavity superflow fields are tightly linked to the steady-state texture. Starting from the dissipation-free hydrodynamics associated with the broken relative spin-orbital-gauge

 0031-9007/99/83(9)/1806(4)$15.00 

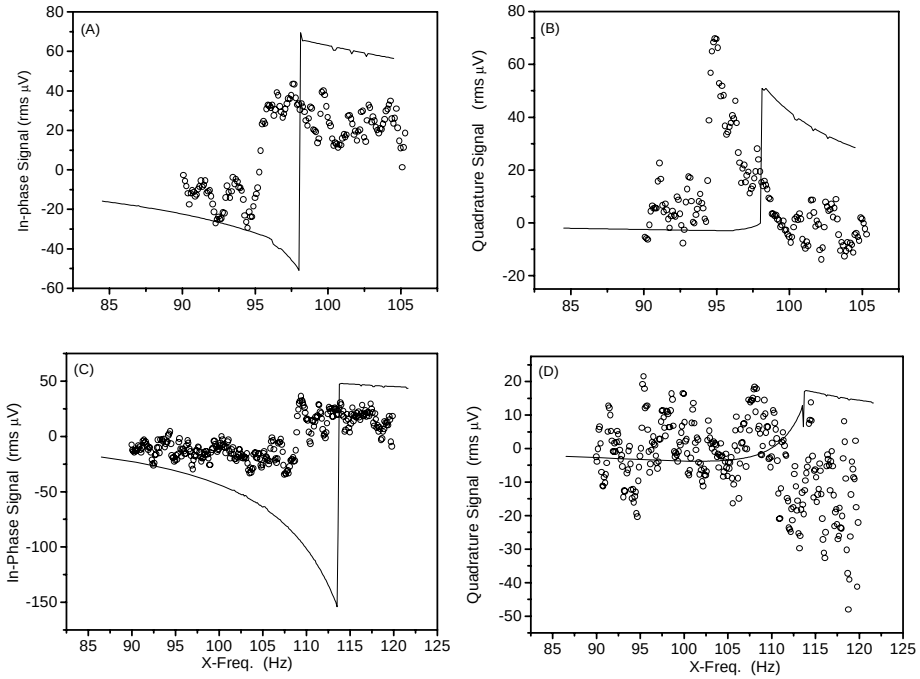


FIG. 1. Panel A (B) shows the in-phase (quadrature) second sound signal at the $x$-pickup transducer as a function of $f_x$ for $x$-drive amplitude ($V_{xdc} = 135$ V, $V_{xac} = 10$ V peak-peak) and no $y$ excitation, below a $y$ jump. Panels C and D present spectra for $y$ drives ($V_{ydc} = 160$ V, $V_{yac} = 4.25$ V peak-peak), measured above a $y$ jump under the same $x$-drive conditions. Open symbols denote experimental data, and the solid lines are the results of simulations for BC(2). The calculations capture the large reduction of the quadrature component above a $y$ jump shown in panel D (note vertical scales).

symmetry of the $A_1$-phase [4], we derived a wave equation describing the propagation of second sound through a given spatially varying texture:

$$\ddot{\mathbf{v}} = (\hbar\gamma/2m)^2/\chi\vec{\nabla}\nabla\cdot(\hat{\rho}_s\mathbf{v}), \tag{1}$$

where $\mathbf{v}$ is the superflow, $\gamma$ is the gyromagnetic ratio of $^3$He, $\chi$ is the magnetic susceptibility, $(\rho_s)_{\alpha\beta} = \rho_{s\parallel}(2\delta_{\alpha\beta} - \hat{\boldsymbol{l}}_\alpha\hat{\boldsymbol{l}}_\beta)$ is the anisotropic superfluid density tensor, and $\rho_{s\parallel} = \rho_{s\perp}/2$. The component of $\mathbf{v}$ perpendicular to the walls vanishes. The $x$ and $y$ transducers, being driven at different frequencies, establish two decoupled, orthogonally polarized, and irrotational velocity fields. The steady-state texture is determined by minimizing the total free energy arising from magnetic susceptibility anisotropy, coherent dipole interaction, $\hat{\boldsymbol{l}}$ gradients, and superflow [1]. $\hat{\boldsymbol{l}}$ is constrained by the magnetic and dipole energies to lie in the $xy$ plane. At interior faces $\hat{\boldsymbol{l}}$ lies perpendicular to the walls. The two boundary conditions (BC) leading to textures of lowest free energy were selected for detailed study. These were BC(1/2) $= [-\hat{\mathbf{x}}(\text{in}), \hat{\mathbf{y}}(\text{out/in}), \hat{\mathbf{x}}(\text{out}), -\hat{\mathbf{y}}(\text{in})]$, where unit vectors designate the outward wall normals, and in and/or out denotes the orientation of $\hat{\boldsymbol{l}}$ at that face. Because the orbital relaxation times of $\hat{\boldsymbol{l}}$ are order of seconds and the counterflow frequencies are near 100 Hz, $\hat{\boldsymbol{l}}$ is unable to follow the instantaneous velocities. Thus the steady-state texture minimizes the total flow and gradient energies averaged over many acoustic cycles. So we numerically search for the planar texture orientation $\theta = \cos^{-1}(\hat{\boldsymbol{x}}\cdot\hat{\boldsymbol{l}})$ which minimizes the dimensionless energy $E$:

$$\delta E[\theta(x,y)]/\delta\theta = 0,$$

where

$$E = \int_{\text{cell}}\langle f/2f_0\rangle\,dx\,dy$$

$$\langle f/2f_0\rangle = (\partial_x\theta)^2[2 + \cos2\theta] + (\partial_x\theta)(\partial_y\theta)\sin2\theta + (\partial_y\theta)^2[2 - \cos2\theta] + (1/2)(1 + 2m^*/3m)(2m/\hbar)^2[v_x^2(3 - \cos2\theta) + v_y^2(3 + \cos2\theta)] \tag{2}$$

for given flow field. $v_x(x,y)$ and $v_y(x,y)$ are the velocity amplitudes established at different frequencies, and $f_0 = (3/16)(m/m^*)(\hbar/2m)^2\rho_{s\parallel}$ [5]. The effective local sound speed in Eq. (1) is $\hat{\boldsymbol{l}}$ dependent, and the $\hat{\boldsymbol{l}}$ texture in turn is affected by the wave's flow fields in Eq. (2). Therefore, we seek self-consistent *steady-state* solutions of Eqs. (1) and (2) given external drive conditions.

To connect with experiment we must compute the amplitude of the cavity flows given drive voltages and frequencies, including cavity dissipation and transducer effects

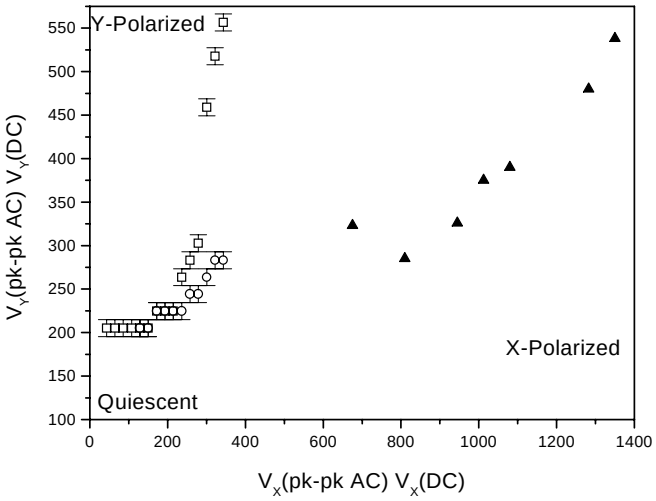


FIG. 2. Textural phase diagram: Solid triangles represent the experimental $(x, y)$ drive conditions for $f_y = 123$ Hz where a $y$ jump was observed in the spectra upon increasing $y$ drive at fixed $x$ drive. Open squares (circles) are numerical results for textural boundary condition 1 (2) at $\rho_s/\rho \approx 4.6 \times 10^{-3}$. Error bars designate the $y$-drive step-size limited resolution.

The dissipationless velocity eigensolution obtained from Eq. (1) is coupled to the drive OST treating it as a localized velocity forcing term, and using the measured cavity $Q$ values to describe a Lorentzian frequency response around the calculated, texture dependent, dissipationless eigenfrequency. This is analogous to coupling an antenna to an electromagnetic cavity field with large $Q$. The OST generates a velocity proportional to the dc bias and ac drive voltages. As previously analyzed in the literature, this superflow is determined by conservation of mass, spin, and entropy flows as the porous membrane oscillates in response to the applied ac electrostatic force between the membrane and a fixed electrode [6]. The OST is described as a quasistatic, massless, undamped piston [7] while imposing continuity of the chemical potential in the condensed spin band [6]. This equivalent piston represents the action of the membrane averaged over its area. The nonequilibrium ac condensed spin density $S$ in the back space generates an ac "spin pressure" on the OST, which in the dissipationless case is larger and acts in addition to the membrane's measured intrinsic tension. Following Liu and Stern, anticipated nuisance effects arising from viscous slip of the normal liquid fraction, normal spin diffusion, and thermal conduction through the OST's pores were all systematically included [6]. Spin diffusion dominates, which *degrades* spin pressure. This *reduces* the membrane's effective spring constant, producing *larger* displacements and larger superflows for given forcing conditions compared to the ideal case, albeit with a phase shift.

Figure 1 displays simulated spectra. We emphasize that there are *no* adjusted parameters [8]. The experimental and computed spectra shown here were selected for their close $x$-resonant frequencies (cell flow velocities). While the simulations capture the overall spectral shapes, the predicted resonant frequencies are off by about 3%. We note that these resonant frequencies are sensitive to $\rho_{s\|}$, leading to considerable temperature dependence. The calculated and measured spectra would match more closely if the $x$-resonant frequencies actually coincided. We computed that the $x$-resonance frequencies increase on crossing a $y$ jump for BC(1) [2] by 12–21 [16–19] Hz depending on $x$ drive. The observed shifts ranged over 3–15 Hz Hz.

Calculated textural phase diagrams are presented in Fig. 2. While they reproduce the form of the observed boundary, the $x$ $(y)$ transducer is a factor of 2–4 (1.5) less effective in the experiments than in our simulations. The model does not include OST internal friction, membrane bowing, $A_1$-phase mutual friction, or more complex superfluid dissipation mechanisms [4].

What is going on at a $y$ jump? Figure 3 shows a computed $\hat{\boldsymbol{l}}$ texture calculated at $f_x = 84.5$ Hz. Panel A (B) is computed just below (above) a $y$ jump. As shown in panel C, the texture initially varies smoothly as the $y$ drive is increased, but upon crossing the $y$ jump $\hat{\boldsymbol{l}}$ explosively aligns along the $y$ direction over most of the cell, accompanied by a free energy discontinuity. The simulated high rms $y$-flow "$y$-polarized state" suddenly created above the $y$ jump displays hysteresis in free energy and orientation of about 90% when $y$ drive is subsequently decreased (not shown). These are hallmarks of a first order transition. The corresponding measured hysteresis is 30%. While this is appreciably smaller than the calculated result, one expects external experimental fluctuations to reduce the range of hysteresis. As shown in panel D, the texture "explodes" when the rms ac $y$ flow ($\sim$2.4 $\mu$m/s) is roughly the $x$ flow ($\sim$1.2 $\mu$m/s). If one nucleates a $y$-polarized texture at low $f_x$ and then sweeps $f_x$ upwards, the $y$-polarized state persists until reaching $x$ resonance, where it violently collapses to a low $y$-flow, high $x$-flow, $x$-polarized state. Flows at such transitions are 2–20 $\mu$m/s, well below measured $A$-phase critical velocities of 2 mm/s [9].

The $x$ drive behaves more tamely at low $y$ excitations. For $f_x = 85$ Hz, as the $x$ drive is increased at constant $y$ drive *below* the transition line, the calculated texture transforms continuously from a low flow, bending dominated configuration into $x$ polarization without abrupt jumps and displays only a hint of hysteresis. This concurs with the observations.

For the bulk case in the presence of ac superflow in the $x$ and $y$ directions at different frequencies, the cycle-averaged kinetic energy is proportional to $3(v_x^2 + v_y^2) - (v_x^2 - v_y^2)\cos(2\theta)$ [1]. This means that $\hat{\boldsymbol{l}}$ prefers to be parallel/antiparallel to the *larger* of the two ac velocities. So a stable equilibrium texture can suddenly transform into an unstable one (and vice versa) upon changing the ac flow conditions. This contrasts with bulk dc flow where kinetic energy is proportional to $(v_x^2 + v_y^2) - (v_x \cos\theta + v_y \sin\theta)^2$, and $\hat{\boldsymbol{l}}$ aligns parallel/antiparallel to the *continuously* varying vector $v_x\hat{\mathbf{x}} + v_y\hat{\mathbf{y}}$. The $y$-jump boundary

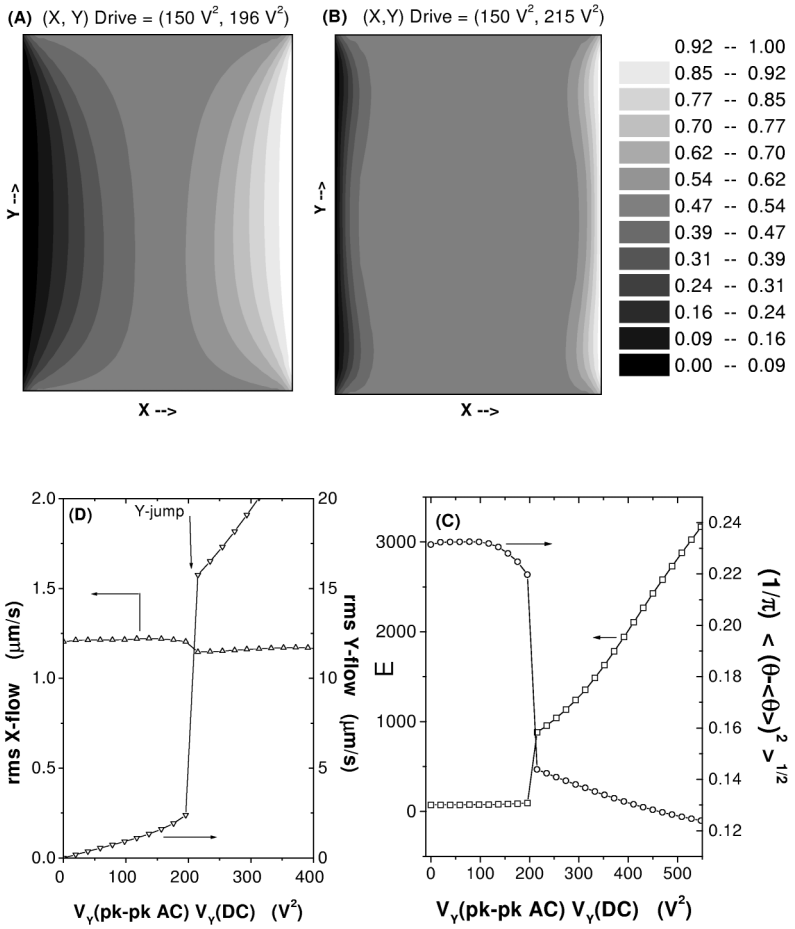


FIG. 3. Panel A (B) displays the computed steady-state texture orientation $\theta/\pi$ just below (above) a $y$ jump for BC(2). Note the sudden polarization of the texture in the $y$ direction over most of the cell. Panel C shows the discontinuous variation of dimensionless free energy $E$ upon crossing the transition. The $y$-drive dependence of the orientation root variance demonstrates that the texture varies smoothly away from the jump. Panel D presents concomitant rms ac flow velocities in the $x$ (up triangles) and $y$ (down triangles) directions.

may then be identified as a first order, nonequilibrium, textural phase transition line. The *steady-state* flows and texture are *discontinuous* functions of the external drive conditions there.

Other research on $\hat{\boldsymbol{l}}$ textures has investigated the effect of dc flow and magnetic fields in the $A$ and $B$ phases, theoretically [1] and experimentally [10]. The interpretation of dc flow experiments is complex and not directly comparable with these results on ac flow in $^3$He-$A_1$.

In conclusion, we have observed and simulated anomalous second sound spectra in a doubly excited resonator filled with superfluid $^3$He-$A_1$. Our simulations account for the measured resonant frequency shifts, line shapes, textural phase diagram, and the first order, hysteretic nature of the transitions. This demonstrates that these observations are the signature of explosive alignment of the $\hat{\boldsymbol{l}}$ texture along the larger of the two perpendicular ac flows.

We thank M. Bastea for cell construction and preliminary studies of the rectangular resonator modes. This research was supported by NSF Grant No. DMR9510306.

*Also at SWK Research, Summit, NJ 07901.
†On leave from Tokyo Institute of Technology and presently at Murata Manufacturing, Kyoto, Japan.

[1] D. Vollhardt and P. Wölfle, *The Superfluid Phases of Helium-3* (Taylor & Francis, London, 1990).
[2] M. Bastea, Y. Okuda, and H. Kojima, Phys. Rev. Lett. **74**, 2531 (1995).
[3] M. Bastea, H. Kojima, and P. G. N. de Vegvar, Phys. Rev. Lett. **76**, 2766 (1996).
[4] M. Liu, Phys. Rev. Lett. **43**, 1740 (1979).
[5] P. G. N. de Vegvar, R. Movshovich, E. L. Ziercher, and D. M. Lee, Phys. Rev. Lett. **57**, 1028 (1986).
[6] M. Liu and M. R. Stern, Phys. Rev. Lett. **48**, 1842 (1982); D. L. Johnson, Phys. Rev. Lett. **49**, 1361 (1982).
[7] M. Liu, Phys. Rev. B **29**, 2833 (1984).
[8] $\rho$, $m^*/m$, $\gamma$, and $\chi$ from J. Wheatley, Rev. Mod. Phys. **47**, 415 (1975), $\rho_{s\|} = \rho_{s\perp}/2$ from $\hat{z}$ mode, membrane tensions, other OST and cavity parameters directly measured.
[9] P. L. Gammel, T. L. Ho, and J. D. Reppy, Phys. Rev. Lett. **55**, 2708 (1985).
[10] H. M. Bozler, in *Helium Three*, edited by W. P. Halperin and L. P. Pitaevskii (North-Holland, Amsterdam, 1990), p. 695; J. R. Hook, *ibid.*, p. 135.